

See discussions, stats, and author profiles for this publication at: <https://www.researchgate.net/publication/275895692>

The Tyrosine Gate of the Bacterial Lectin FimH: A Conformational Analysis by NMR Spectroscopy and X-ray Crystallography

ARTICLE *in* CHEMBIOCHEM · MAY 2015

Impact Factor: 3.09 · DOI: 10.1002/cbic.201402714 · Source: PubMed

READS

36

9 AUTHORS, INCLUDING:



Brigitte Fiege

University of Basel

8 PUBLICATIONS 200 CITATIONS

[SEE PROFILE](#)



Said Rabbani

University of Basel

33 PUBLICATIONS 632 CITATIONS

[SEE PROFILE](#)



Roman P Jakob

University of Basel

23 PUBLICATIONS 354 CITATIONS

[SEE PROFILE](#)



Oliver Schwardt

University of Basel

53 PUBLICATIONS 1,052 CITATIONS

[SEE PROFILE](#)

VIP

The Tyrosine Gate of the Bacterial Lectin FimH: A Conformational Analysis by NMR Spectroscopy and X-ray Crystallography

Brigitte Fiege,^[a] Said Rabbani,^[a] Roland C. Preston,^[a] Roman P. Jakob,^[b] Pascal Zihlmann,^[a] Oliver Schwardt,^[a] Xiaohua Jiang,^[a] Timm Maier,^{*[b]} and Beat Ernst^{*[a]}

Urinary tract infections caused by uropathogenic *E. coli* are among the most prevalent infectious diseases. The mannose-specific lectin FimH mediates the adhesion of the bacteria to the urothelium, thus enabling host cell invasion and recurrent infections. An attractive alternative to antibiotic treatment is the development of FimH antagonists that mimic the physiological ligand. A large variety of candidate drugs have been developed and characterized by means of in vitro studies and animal models. Here we present the X-ray co-crystal structures of FimH with members of four antagonist classes. In three of these cases no structural data had previously been available.

We used NMR spectroscopy to characterize FimH–antagonist interactions further by chemical shift perturbation. The analysis allowed a clear determination of the conformation of the tyrosine gate motif that is crucial for the interaction with aglycone moieties and was not obvious from X-ray structural data alone. Finally, ITC experiments provided insight into the thermodynamics of antagonist binding. In conjunction with the structural information from X-ray and NMR experiments the results provide a mechanism for the often-observed enthalpy–entropy compensation of FimH antagonists that plays a role in fine-tuning of the interaction.

Introduction

Urinary tract infection (UTI) is one of the most frequent infectious diseases, affecting millions of people every year.^[1] Women have a 50% risk of experiencing at least one symptomatic UTI during their lifetime. The large majority of UTIs are caused by uropathogenic *Escherichia coli* (UPEC) that are able to invade the urothelial cells in the bladder, form biofilms, and cause recurrent infections.^[2] To date, UTIs are mainly treated with antibiotics, thus inducing antimicrobial resistance, a serious threat to patients worldwide.^[3] Therefore, new treatment strategies are urgently needed.

Adherence of UPEC to the urothelial surface is mediated through the mannose-specific lectin FimH, located at the tip of bacterial type 1 pili.^[4] FimH therefore represents a major virulence factor of UPEC. It consists of two immunoglobulin-like domains: the N-terminal lectin domain, or carbohydrate recognition domain (CRD), and, connected by a short linker, the C-terminal pilin domain. The pilin domain anchors the adhesin to the pilus and regulates the switch between the two conforma-

tional states—with either high or low affinity for mannosides—of the CRD.^[5] Most in vitro interaction studies with FimH antagonists have been performed only with the lectin domain FimH-CRD that is trapped in the high-affinity state.^[6]

The natural ligand for FimH is the mannosylated glycoprotein uroplakin Ia present on urothelial cells.^[7] Mannose-based FimH antagonists compete with this interaction and prevent bacterial adhesion and hence infection. A substantial advantage of this anti-adhesion therapy over antibiotics treatment is the reduced risk of resistance development, because no direct selection pressure is imposed on the pathogen.^[8] The first successful demonstration of the anti-adhesion strategy was of the protective effect of methyl α-D-mannoside in a UTI mouse model.^[9] Since then, significant progress has been made in the optimization of FimH antagonists, yielding improved affinities in the low nanomolar range.^[10]

In part, these modifications are the result of rational drug design based on X-ray crystal structures of FimH bound to various α-D-mannosides.^[11] The mannose moiety is in each case tightly bound and involved in an extended hydrogen bond network. A promising prospect for optimizing binding is offered by a rim of hydrophobic residues lining the entrance to the mannose pocket. This so-called tyrosine gate, consisting of Tyr48 and Tyr137, with Ile52 positioned in-between, is involved in interactions with oligomannosides, as revealed by the X-ray co-crystal structure of FimH-CRD with oligomannose-3.^[12] For drug design, the tyrosine gate has been exploited for hydrophobic stacking interactions with suitable aglycones. In particular, the finding that mannosides with hydrophobic aryl and

[a] Dr. B. Fiege, Dr. S. Rabbani, Dr. R. C. Preston, P. Zihlmann, Dr. O. Schwardt, Dr. X. Jiang, Prof. B. Ernst
Institute of Molecular Pharmacy, University of Basel
Klingelbergstrasse 50, 4056 Basel (Switzerland)
E-mail: beat.ernst@unibas.ch

[b] Dr. R. P. Jakob, Prof. T. Maier
Structural Biology, Biozentrum, University of Basel
Klingelbergstrasse 70, 4056 Basel (Switzerland)
E-mail: timm.maier@unibas.ch

 Supporting information for this article is available on the WWW under <http://dx.doi.org/10.1002/cbic.201402714>.

alkyl aglycones show stronger affinities has led to many promising drug candidates. Through binding studies with a series of alkyl mannosides, *n*-heptyl α -D-mannoside (**1**, Table 1, below) was identified as the most efficient non-aromatic FimH binder.^[11a] For aryl and heteroaryl derivatives a large variety of antagonists differing in the number of aromatic rings and substituents and the type of linkers exist. Chemically easily accessible aromatic derivatives such as 4-nitrophenyl and 4-methyl-umbelliferyl mannosides were soon discovered.^[11a,13] These were followed by derivatives of squaric acid,^[14] biphenyls and other diaryls,^[15] triazoles,^[16] and indolines,^[17] among others.

We routinely test new candidates for in vitro binding to FimH-CRD^[15b,16–18] and to UPEC,^[19] as well as for efficacy in a UTI mouse model.^[20] A special focus is placed on the PK/PD (pharmacokinetic/pharmacodynamic) properties for oral bioavailability.^[21] The ideal FimH antagonist for UTI treatment needs to be balanced between a reasonable solubility for effective dosage and a certain degree of lipophilicity for efficient membrane permeation during oral absorption. Despite the availability of structural information, rational design of FimH antagonists has not always led to the expected improvement in binding affinities. Specifically, thermodynamic profiles from isothermal titration calorimetry (ITC) have frequently revealed enthalpy–entropy compensations,^[15d,21] the reasons for which are not yet fully understood.

In this study, we analyzed the binding of a representative set of FimH antagonists to FimH-CRD by means of a combination of high-resolution X-ray crystal structures and NMR chemical shift perturbation (CSP) experiments. NMR spectroscopy allows the study of protein–carbohydrate interactions in solution, with the native dynamic behavior of the protein thus being maintained.^[22] In contrast, X-ray crystallography provides structural information from a “static” crystal with limited information on flexibility. The two methods are therefore highly complementary.

The potential of NMR spectroscopy to contribute to the drug design process has been widely acknowledged.^[23] The chemical shifts of protein resonances are highly sensitive to the chemical environment, for example to hydrogen bonds and aromatic ring currents.^[24] CSP effects hence identify residues in direct proximity to a bound ligand and, in addition, indicate conformational changes in allosteric sites. We used ^1H , ^{15}N HSQC experiments with ^{15}N -enriched FimH-CRD in the presence of various antagonists to monitor the CSP effects on the backbone amide groups. Previous NMR studies of binding of methyl α -D-mannoside^[6] and *n*-heptyl α -D-mannoside^[25] to FimH-CRD only noted a general match of the CSP maps and the ligand binding interface identified from X-ray co-crystal structures. With our analysis we demonstrate that NMR and X-ray structural data can be combined to characterize FimH-antagonist complex formation in unprecedented detail. In addition to the structural information, ITC experiments were performed to quantify the thermodynamics of antagonist binding to FimH-CRD.

Results and Discussion

FimH antagonist classes studied in this work

In this study we examined FimH antagonists composed of an α -D-mannosyl residue linked to an aliphatic or aromatic aglycone (Table 1). *n*-Heptyl α -D-mannoside (**1**)^[11a] is the only non-aromatic antagonist with an affinity (low nanomolar range)

Table 1. FimH antagonists analyzed for binding to FimH-CRD by X-ray crystallography (PDB ID and reference for reported structures given) and/or CSP NMR experiments (indicated with +).

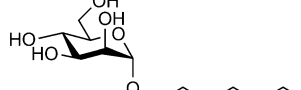
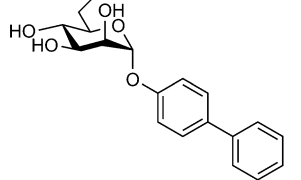
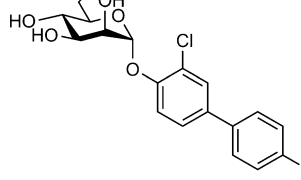
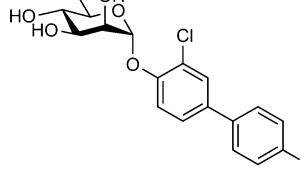
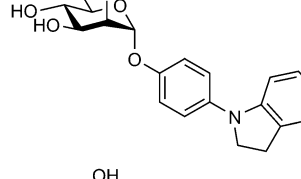
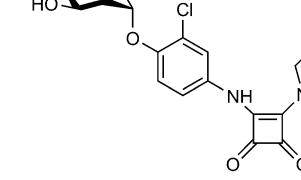
Compd	Structure	X-ray	NMR
1		4BUQ ^[27]	+
2		4X50	+
3		n.d.	+
4		4CST ^[21]	+
5		4X5Q	+
6		4X5R	+

Table 1. (Continued)

Compd	Structure	X-ray	NMR
7		4X5P	+
8		n.d.	+
9		1UWF, 1TR7 ^[11a]	+
10		n.d.	+
11		n.d.	+

similar to those of the aromatic antagonists **2** to **7** (Table 1 and Table 2, below). Although its pharmacokinetic properties render **1** ineffective for oral administration, it is often used as a reference compound in screening studies. Biphenyl mannoside **2**^[15a] was rationally designed to form aromatic stacking interactions with the side chains of Tyr48 and Tyr137 in the tyrosine gate. Later on, the aryl moieties were derivatized to optimize this interaction, as reported by our group and others.^[15] An impressive example of this is represented by biphenyl mannoside **4**, with an *ortho*-chloro substituent on the inner aromatic ring and a cyano group in the *para* position of the outer ring as a bioorthogonal replacement for the carboxylate group present in antagonist **3**.^[21] Both ring substituents of **4** reduce the electron density in the aglycone and thereby enhance the π - π interaction, thus leading to a more than tenfold affinity improvement relative to the unsubstituted antagonist **2** (Table 2, below). Besides the biphenyls **2** to **4**, three other compound classes with multiple aromatic rings in nonplanar arrangements have been tested: **5** features a 5-nitroindolinyl moiety *N*-linked to an inner phenyl ring,^[17] **6** extends an *ortho*-chlorophenyl system with squaric acid and *N*-methyl-piperazine,^[14b] and in **7** (for synthesis see the Supporting Information) an amide bond is inserted between two phenyl rings with *ortho*-chlorine and *para*-carboxylate substituents.

In addition to high-affinity antagonists, we also studied methyl α -D-mannoside (**8**), *n*-butyl α -D-mannoside (**9**), and 1,5-anhydromannitol (**10**). Finally, the 4-deoxy-4-fluoro derivative **11** (for synthesis see the Supporting Information) exhibits a dramatically reduced affinity relative to **1**, emphasizing the impor-

tance of the hydrogen bond network in the mannose binding pocket.

X-ray crystal structures of FimH with antagonists

We obtained high-resolution X-ray structures of FimH-CRD co-crystallized with antagonists **2** and **5–7**, with resolutions ranging from 1.00 to 2.00 Å (Table 1 and Table S1 in the Supporting Information), and compared them with the reported structures with antagonists **1** and **4**.^[21] FimH-CRD consists of eleven mainly antiparallel β -strands and two short helices (Figure 1).

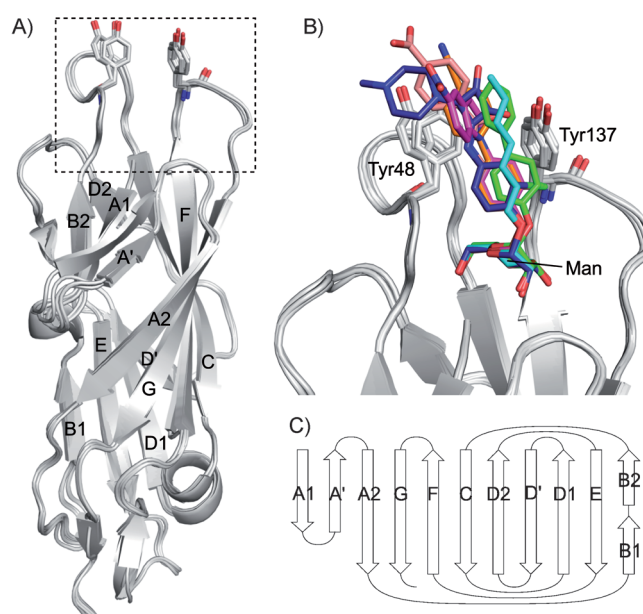


Figure 1. Superposition of X-ray co-crystal structures of FimH-CRD with six antagonists: A) only protein is shown, with Tyr48 and Tyr137 as gray sticks, and B) with antagonists shown as colored sticks (1 cyan, 2 green, 4 orange, 5 magenta, 6 blue, and 7 salmon). C) β -sheet topology diagram of FimH-CRD.^[11a,29]

Superposition of the six protein structures reveals a high structural similarity with a backbone RMSD of around 0.5 Å between any two structures. In all six structures the ligand is bound within the mannose binding pocket. The mannose moieties form hydrogen bonds to the side chains of residues Asp54, Gln133, Asn135, and Asp140 and to the backbone atoms of Phe1 and Asp47 (Figure S1). Tyr48 is involved in stacking interactions with the outer aromatic ring of the aglycones or, in the case of **1**, with the alkyl chain of the ligand (Figure 1). Tyr137 stabilizes the loop containing Tyr48 through a hydrophobic interaction with Ile52. In the cases of **6** and **7**, the side chain hydroxy group of Tyr137 can form a hydrogen bond with the oxygen atoms of the squaric acid and the amide bond, respectively. Moreover, the backbone amide groups of Tyr137, Asn138, and Asp140 and the side chains of Asn135, Asn138, and Asp140 form a complex hydrogen bond network within the loop and with the 3- and 4-positions of the mannose residues of the ligands.

It is noteworthy that in all six structures the side chain of tyrosine gate residue Tyr137 has a single orientation whereas Tyr48 shows two slightly different orientations. In all cases, the side chain positions correspond to the *closed conformation* of the tyrosine gate as described previously.^[11a, 15a, d, 26] The *closed* conformation was also observed in co-crystal structures of FimH-CRD with *n*-butyl α -D-mannoside (**9**) (PDB ID: 1UWF)^[11a] or with a biphenyl mannoside with a methylcarboxylate group in the *meta*-position of the outer aromatic ring (PDB ID: 3MCY).^[15a]

A significantly different orientation of the tyrosine gate, termed the *open conformation*, was observed in the crystal structure of the full-length FimH in complex with α -D-mannose stabilized by the chaperone FimC (PDB ID: 1KLF),^[11b] and of FimH-CRD with ethane-1,2-diol in the mannose binding site (PDB ID: 4AUU).^[26] The latter is considered a “pseudo-apo” structure, although the bound ethane-1,2-diol could still have an influence on the binding site. Whereas the Tyr137 side chain in these structures remains in the orientation seen in the *closed* conformation, the Tyr48 side chain is rotated towards the mannose pocket by about 3.5 Å. This *open* conformation of FimH-CRD was also observed in the co-crystal structure with the native ligand epitope oligomannose-3, Man α 1,3(Man α 1,6)-Man β 1,4GlcNAc β 1,4GlcNAc (PDB ID: 2VCO).^[12] Here, the α 1,3-linked mannose at the nonreducing end is recognized in the orientation typical for all mannosides. This brings the first GlcNAc residue into a position in which it would clash with Tyr48 in the *closed* conformation. In view of the limited conformational freedom around the glycosidic linkages, it can be speculated that oligomannose-3 might only be able to bind to FimH in the *open* conformation.

In computational studies, FimH antagonists with flexible aglycones have been docked to FimH in both conformations of the tyrosine gate.^[11a, 15d] As an experimental verification, *n*-butyl α -D-mannoside (**9**)^[11a] and several monoaryl antagonists^[27] have been co-crystallized with FimH-CRD in both the open and the closed forms. Wellens et al. proposed that the *open* conformation represents the minimum-energy conformer of FimH and that the *closed* conformation is only stabilized by favorable interactions with hydrophobic aglycones.^[26] This would correspond to a conformational selection process in which the ligand binds to a conformer from a preexisting set of substates.^[28] Nevertheless, an induced-fit mechanism also seems possible.

To conclude, Tyr48 can be regarded as a key element in ligand interaction, and knowledge of the Tyr48 side chain conformation is critical to the discussion. Unfortunately, in many FimH-mannoside co-crystal structures the binding pocket residues or the ligand are involved in crystal lattice contacts potentially affecting the binding pocket geometry.^[26–27] Therefore, more experiments are needed to study the structure and dynamics of FimH-antagonist complex formation in solution.

NMR experiments with FimH-CRD

We performed NMR experiments to obtain structural information on FimH-antagonist complexes in solution. This allows full

retention of the molecule dynamics and avoids potential distortion from crystal packing. The binding of antagonists to ^{15}N -labeled FimH-CRD (173 residues) was monitored by CSP analysis of ^1H , ^{15}N HSQC fingerprint spectra representing the backbone amide groups. For efficient affinity purification, the protein contained a C-terminal His₆-tag, which does not influence mannoside binding.^[18] A complete backbone resonance assignment was performed by measuring a set of triple-resonance NMR spectra with a ^{13}C , ^{15}N -labeled FimH-CRD sample. The high chemical shift dispersion of the amide resonances allowed sequential backbone assignment mainly on the basis of HNCACB and CBCACONH spectra.^[30] A total of 152 (94.4%) out of 161 assignable residues were assigned.^[31] The His₆-tag remained unassigned. Three residues were absent in the ^1H , ^{15}N HSQC spectrum: the backbone and side chain signals of Asn96 and Arg98, which are located in a loop close to the binding pocket, as well as Gly79, which is located in a solvent-exposed loop about 20 Å away from the binding pocket. Carbon and proton signals of the side chains of these three residues were observed as (*i*–1) correlations of the succeeding residues, thus suggesting that fast exchange with the solvent and not (solely) conformational exchange was responsible for the absence of signals. The assignment matches that from a recently published study of FimH-CRD (BMRB entry: 19066)^[25] that lacked a His₆-tag. Those authors were able to observe and assign Gly79, Asn96, and Arg98 amide signals. This is likely due to different measuring conditions, in particular a lower pH of 6.0,^[25] in comparison with pH 6.8 (for assignment) and pH 7.0 (for CSP experiments) in this study.

Chemical shift perturbation experiments: We subjected ^{15}N -labeled FimH-CRD to CSP experiments with antagonists **1** to **11** (Table 1). Methyl α -D-mannoside (**8**) and *n*-heptyl α -D-mannoside (**1**) have been analyzed in similar studies before.^[6, 25] With all compounds, separate signals for the bound and free forms were observed in the ^1H , ^{15}N HSQC spectra at 500 MHz, thus indicating slow exchange on the NMR timescale. The observation is in accordance with nanomolar to low micromolar affinities (Table 2) and with kinetic data obtained from surface plasmon resonance experiments.^[32] Interestingly, even antagonist **11**, which binds to FimH-CRD with a greatly diminished affinity of 83 μM (Table 2), was found to be in slow or intermediate exchange. Slow exchange kinetics might suggest rearrangements of conformation during complex formation.

For the non-overlapping signals in the ^1H , ^{15}N HSQC spectra, combined chemical shift changes ($\Delta\delta_{\text{AVG}}$) with respect to the protein signals in the absence of ligand were determined (Figure 2A). 1,5-Anhydromannitol (**10**) is the smallest structural motif that still shows specific binding to the mannose pocket of FimH-CRD. Its CSP effects were therefore used to calculate differential CSP effects ($\Delta\Delta\delta_{\text{AVG}}$) for the other ligands that should mainly reflect the influence of the aglycone moieties (Figure 2B and C). In the presence of antagonists **1** to **11**, FimH-CRD displayed chemical shift changes for residues near the known mannose binding site. Only minor CSP effects of below 0.1 ppm were observed for residues distal from this site. Because proton chemical shifts are highly sensitive to changes in hydrogen bond length,^[24] global conformational changes of

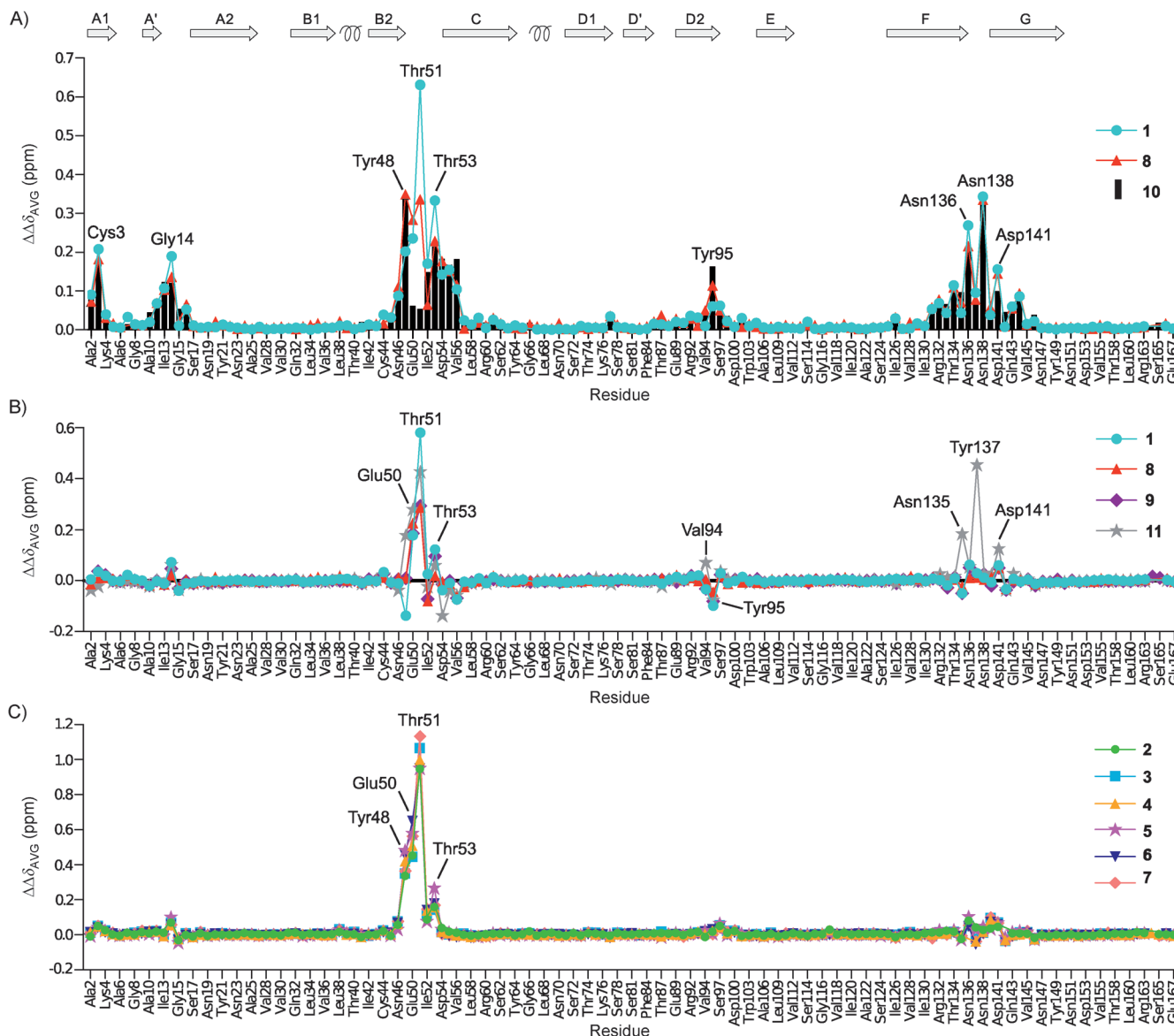


Figure 2. Chemical shift changes of FimH-CRD backbone amide signals upon addition of FimH antagonists. A) Absolute combined chemical shift changes ($\Delta\delta_{AVG}$) of 1, 8, and 10. B, C) Differential CSP effects ($\Delta\Delta\delta_{AVG}$) of B) aliphatic, and C) aromatic ligands relative to 1,5-anhydromannitol (10). Secondary structure elements are schematized on top. Residues missing from the chart are Phe1 (N terminus), 11 proline residues (residues 12, 26, 49, 83, 85, 91, 102, 104, 111, 157, and 162), Gly79, Asn96 and Arg98 (not observed), Asp47, Tyr108 and Phe142 (overlap), Ser139 (exchange broadening), as well as the C-terminal His₆-tag (residues His168 to His173).

FimH-CRD in response to antagonist binding can be excluded, in view of the fact that the protein is mainly composed of anti-parallel β -sheets that form numerous hydrogen bonds.^[29] The observation is in agreement with the high structural similarity of the X-ray co-crystal structures discussed above. In presence of the “core” motif 10, significant $\Delta\delta_{AVG}$ values, above 0.1 ppm, were observed for (in order of decreasing $\Delta\delta_{AVG}$) Tyr48, Asn138, Thr53, Asn136, Asp54, Val56, Cys3, Tyr55, Asp47, Tyr95, Ile52, Ile13, Gly14, Thr134, and Asn46. Most of these residues directly constitute the binding pocket, in particular residues from the loop regions between β -sheets A' and A2 (Ile11 to Gly16), B2 and C (Asn46 to Val56), and F and G (Arg132 to Phe144). Of these, Tyr48, Ile52, and Tyr137 form the tyrosine gate that is known to interact with the aglycone moieties of

FimH antagonists. In addition, CSP effects were observed for residues Ala2 and Cys3, located at the bottom of the binding pocket, and for Tyr95, which forms a hydrogen bond with the pocket residue Asp54. For most residues, only very small $\Delta\Delta\delta_{AVG}$ values were observed. Larger deviations were observed for loop residues around Tyr137 in the presence of 11 (see later discussion) and for loop residues around Tyr48.

CSP data report on the Tyr48 side chain conformation: The strongest and most heterogeneous chemical shift changes of FimH-CRD with different antagonists were observed for the loop residues Tyr48, Glu50, Thr51, Ile52, and Thr53 (Figures 2 and 3). In the X-ray structures of FimH-CRD co-crystallized with 1, 2, and 4 to 7, the Tyr48 side chain directly interacts with the aglycone moieties and adopts an orientation significantly dif-

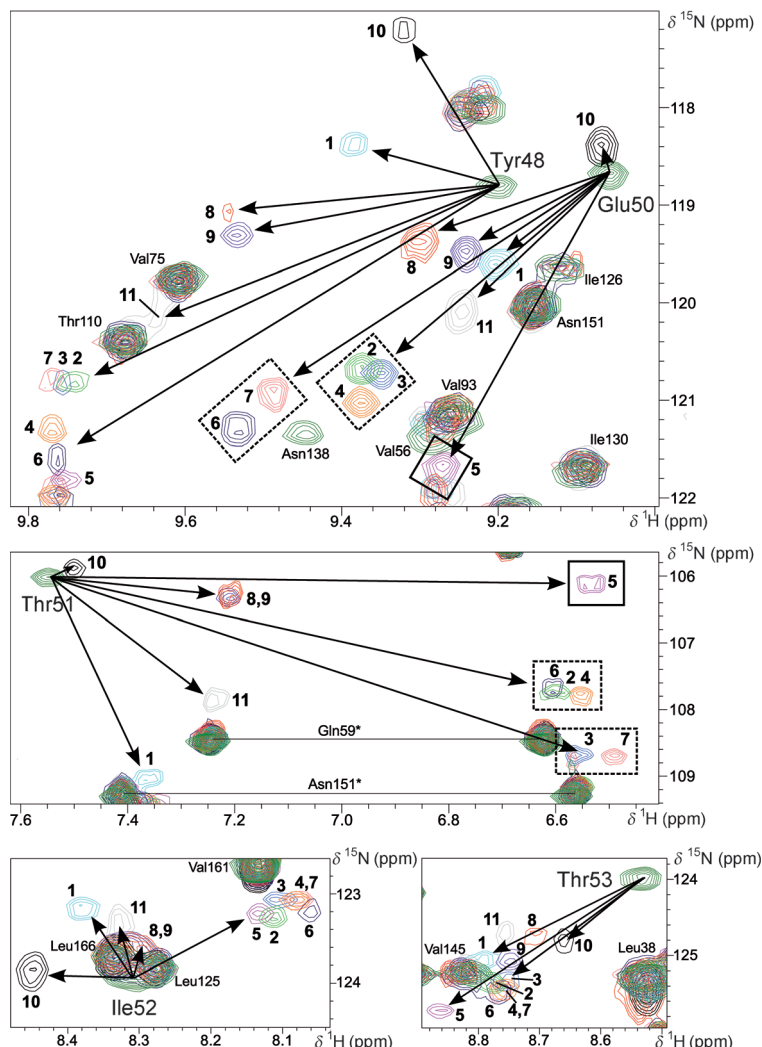


Figure 3. Chemical shift changes of the binding loop residues Tyr48, Glu50, Thr51, Ile52, and Thr53 in the presence of antagonists **1** to **11**. Spectra in absence of ligand are colored in green. Signals corresponding to Tyr48 conformations *a* and *b* in Figure 4 are marked by dashed and solid line boxes, respectively.

ferent from that observed in the “pseudo-apo” X-ray structure^[26] and in a recently solved NMR solution structure^[25] (Figure S2). Apart from Tyr48, the conformation of the loop residues is remarkably conserved in all FimH-CRD crystal structures. This includes hydrogen bonds between Tyr48 H^N and Asn46 O^{δ1}, between Glu50 H^N and its side chain oxygen (stabilized by interaction with the guanidinium group of Arg98, Figure S3), and between Thr51 H^N and Tyr48 O. We hypothesized that the observed backbone CSP effects of Tyr48 to Thr53 mainly reflect the change in conformation of the Tyr48 side chain rather than direct ligand effects. In general, aromatic rings dramatically influence the chemical shifts of nearby nuclei through the local magnetic fields induced by their delocalized π electrons. For protons located on the outside of the ring, the local magnetic field is parallel to the external field, causing a downfield shift (higher ppm values). In contrast, protons located inside or above the ring experience an opposing field and hence an upfield shift. For Tyr48 and Glu50, we ob-

served strong downfield shifts of both proton and ¹⁵N chemical shifts in the presence of antagonists, whereas Thr51 experienced a strong proton upfield shift of up to 1 ppm and above (Figure 3). The shifts were larger for aromatic aglycones than for aliphatic ones. In the *open* conformation seen in the “pseudo-apo” crystal structure^[26] the Tyr48 ring is distant from the loop residues. In the *closed* conformation, it is rotated towards the loop such that Glu50 H^N comes closer and within 30° of the ring plane, where it experiences a strong deshielding aromatic ring current. In contrast, Thr51 H^N points almost directly into the ring in a T-shaped orientation in which a strong shielding field causes upfield shifts.^[33] Previous studies had demonstrated that T-shaped N–H···π interactions can significantly contribute to ligand binding affinities.^[34] Enhancement of the aromatic ring current effect through π–π stacking provides the explanation for the generally larger CSP effects observed for aromatic antagonists than for their aliphatic counterparts. Importantly, Glu50 and Thr51 show almost no shifts in the presence of **10**; this strongly indicates that FimH-CRD remains in the unperturbed *open* conformation.

A more detailed analysis of the CSP effects with aromatic antagonists allows even further differentiation of the Tyr48 orientation in the *closed* conformation. The signals of Glu50 and Thr51 are grouped together in the presence of compounds **2**, **3**, **4**, **6**, and **7** (Figure 3, dashed line boxes). With antagonist **5**, slightly different shifts were observed, thus suggesting a different orientation of Tyr48. Aliphatic compounds **1** and **8–11** cannot be directly compared to the aromatic antagonists, because the aromatic ring current effect of Tyr48 as the main source of the shifts is drastically different. In good agreement with the NMR results, the high-resolution X-ray structure of FimH-CRD in complex with **5** shows a distinct orientation of the Tyr48 ring, which is tilted by about

40° in relation to the co-crystal structures with compounds **1**, **2**, **6**, and **7** (Figure 4, bottom). This tilt is likely the result of the unique geometry of the nonplanar indolinylphenyl moiety of **5** and the propensity of the system to optimize the stacking interaction. Interestingly, in the co-crystal structure with biphenyl derivate **4** the electron density clearly allows positioning of the Tyr48 ring in both conformations (Figure 4). We cannot find any confirmation for this in the NMR experiments, because only a single set of bound signals is observed with **3** and the CSP effects are very similar to those with compounds **2** and **6** with a single Tyr48 orientation in the crystal structure. Nevertheless, it is conceivable that Tyr48 could retain a certain degree of flexibility in the bound state (see later discussion on ITC data). NMR chemical shifts of the binding loop residues thereby would show an average of rapidly exchanging Tyr48 orientations in the complex.

Water coordination in the FimH binding pocket: Some CSP effects are expected to be due to direct interactions of the pro-

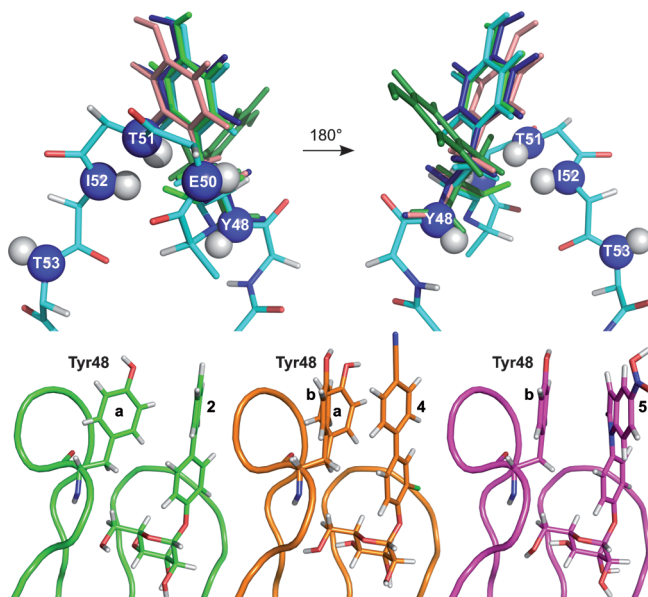


Figure 4. Orientation of the Tyr48 side chain in FimH-CRD crystal structures. Top: Loop residues Tyr48 to Thr53 in the co-crystal structure with **1** (backbone in cyan, amides shown as spheres); Tyr48 side chain in the “pseudo-apo” structure^[26] (green) and with **1** (cyan), **2** (pale green), **6** (dark blue), and **7** (salmon). Bottom: Different Tyr48 orientations (a and b) with **2**, **4** and **5**.

tein with the mannosyl moiety. X-ray structural data implicate the formation of a direct hydrogen bond between Asp47 H^N and Man OH6 and of a water-mediated hydrogen bond between Gly14 H^N and Man OH2 (Figure 5). Against the expectation of a ¹H downfield shift from deshielding upon hydrogen bond formation, both amide protons showed upfield shifts (Figure 5). This instead points to weakening of an existing hydrogen bond. Although other more complex effects cannot be excluded, the results indicate that Gly14 and Asp47 coordinate water in the absence of ligand, and that upon mannose binding this is replaced by polar groups of the ligand in an effectively weaker hydrogen bond. The higher degree of freedom of water molecules might indeed allow hydrogen bonds with more ideal geometries than in the ligands. In the X-ray co-crystal structures with antagonists **1**, **2**, and **4** to **7** the distances between the bridging water and Gly14 H^N are 0.1 to 0.2 Å less than in the “pseudo-apo” crystal structure, in agreement with our hypothesis (Figure 5). Finally, molecular dynamics simulations also indicated the presence of a structural water molecule close to Gly14.^[35]

Hydrogen bond network in the binding loop with Tyr137: The loop residues Asn135 to Asp141 display similar CSP effects in the presence of all tested antagonists except **11** (Figure 2). X-ray co-crystal structures revealed a complex interresidue hydrogen bond network between backbone and side chain atoms within this loop (Figure 6). Asn138 H^N, for example, forms a hydrogen bond to the side chain oxygen of Asn135. The strong deshielding of Asn138 H^N in the presence of ligand suggests a strengthening of this hydrogen bond (Figure 6). The shift could also be the result of a change in the conformation of the aromatic ring of Tyr137. However, Tyr137 H^N displayed no or only very small shifts, thus suggesting that its aromatic ring

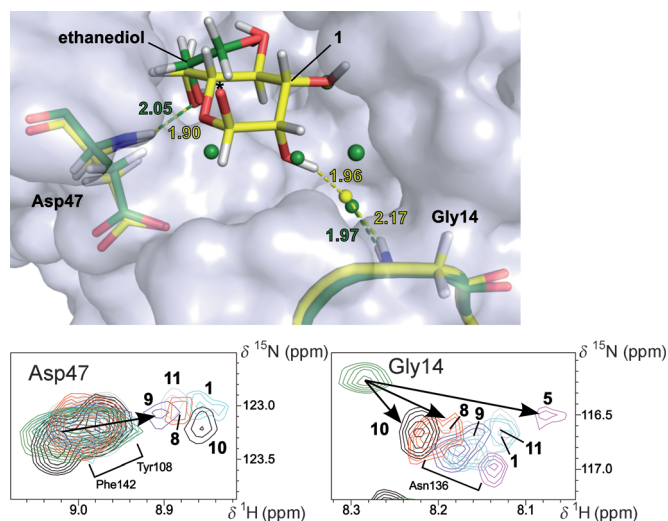


Figure 5. Water coordination in the FimH binding pocket. Top: X-ray structures of “pseudo-apo” FimH-CRD (with ethane-1,2-diol in the binding pocket, green sticks and transparent surface)^[26] and in complex with **1** (yellow, asterisk indicates attachment point of aglycone); water molecules are shown as spheres, and hydrogen bond lengths are given in Å. Bottom: Chemical shift changes of Asp47 (only assigned for nonaromatic antagonists) and Gly14 (only subset of spectra shown).

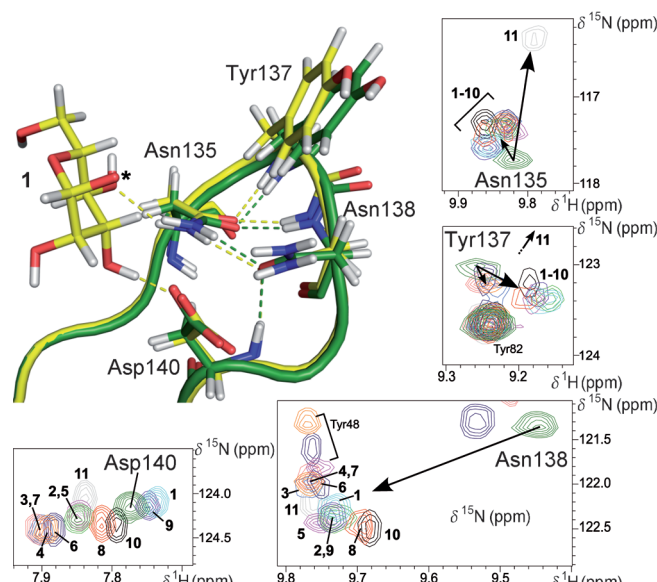


Figure 6. Hydrogen bond network in the binding loop with Tyr137. Top left: X-ray crystal structures of “pseudo-apo” FimH-CRD (green)^[26] and in complex with **1** (yellow, attachment point of aglycone marked with an asterisk). Observed hydrogen bonds: Asn135 H^N...Asn138 O^{δ1}, Tyr137 H^N...Asn135 O^{δ1}, Asn138 H^N...Asn135 O^{δ1}, and Asp140 H^N...Asn138 O^{δ1}. With ligand: Man O-H...Asp140 O^{δ1} and Asn135 H^N...Man O4. Bottom and right: Chemical shift changes of Asn138 and Asp140 with antagonists **1** to **11**.

remains largely unchanged, in agreement with very similar orientations in the X-ray structures. Furthermore, deshielding of Asp140 H^N with all ligands except **1** and **9** indicates a slight shortening of the hydrogen bond to the side chain oxygen of Asn138 (Figure 6).

In summary, mannose coordination seems to induce subtle but specific conformational changes in the hydrogen bond network within the binding loop. The differences in the CSP effects of Asn135, Tyr137, and Asp141 with the 4-deoxy-4-fluoro derivate **11** are hence caused by a different electronic environment of the fluorine atom that also imposes a different loop arrangement through disruption of hydrogen bonds. The X-ray structural data are not entirely conclusive on the effect of mannose binding to the loop conformation. In all six co-crystal structures discussed above, the loop residues are well ordered, but hydrogen bonds in the loop are identical within error to those in the “pseudo-apo” structure. Apparently, very small conformational changes, notably in a solvent-exposed loop with low-populated fluctuating states, cannot be captured by X-ray crystallography.

Conformational changes in the pocket zipper motif: The CSP effects for Cys3 are unlikely to be caused by direct ligand effects, in view of its remoteness ($>8.5\text{ \AA}$) from the bound mannose. In FimH-CRD, Cys3 is part of a highly structured and stable hydrogen bond network to neighboring β -strands further stabilized by a disulfide bond to Cys44 (Figure 7). This so-

crystal structures discussed above, the hydrogen bond between Cys3 H^{N} and Ile11 O is 0.2 to 0.3 \AA shorter than in the “pseudo-apo” structures, in agreement with the CSP effects (Figure 7). Such a difference is considered to be significant at the given resolution.^[37] A strengthening of the “pocket zipper” upon ligand binding could point to a residual conformation transition of FimH-CRD. However, no CSP effects were observed in the other allosteric regions, thus confirming that the isolated lectin domain is not undergoing significant conformation adaptions characteristic of the full-length protein. Corresponding NMR solution studies of full-length FimH would be highly desirable but have so far been hampered by limited protein yield and stability.

Thermodynamics data from ITC experiments

FimH antagonists **1** to **11** have been subjected to thermodynamic profiling by ITC analysis with FimH-CRD (Table 2 and Table S2). To obtain reliable thermodynamics data, the high affinities of some of the compounds required the establishment of a competitive ITC assay^[38] (see the Supporting Information).

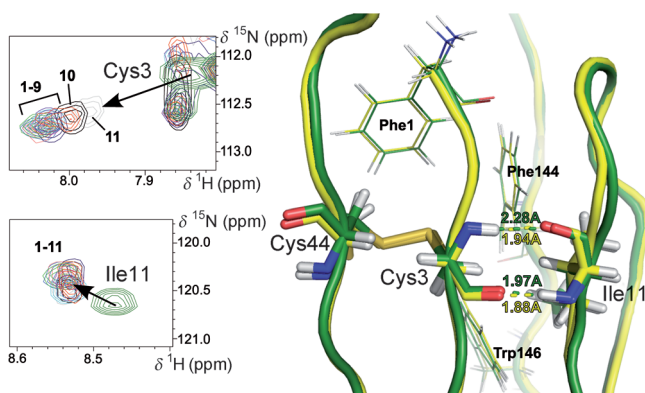


Figure 7. Conformational changes in the pocket zipper motif. Left: Chemical shift changes of Cys3 and Ile11 in the presence of **1** to **11**. Right: X-ray crystal structures of “pseudo-apo” FimH-CRD (green)^[26] and in complex with **1** (yellow); hydrogen bond lengths are given in \AA , and aromatic residues in the vicinity are shown as lines.

called “pocket zipper” motif is one of four regions that are suspected to play a key role in the conformation transition between the low- and the high-affinity states in the full-length FimH.^[6,36] Upon transition to the high-affinity state, the “pocket zipper” becomes tightly hydrogen bonded, causing a constriction of the binding pocket.^[6] The isolated lectin domain FimH-CRD is believed to be locked in the high-affinity state. In the CSP experiments with FimH antagonists, we observed relatively uniform downfield shifts for Cys3 H^{N} , which forms a hydrogen bond to the backbone oxygen of Ile11 (Figure 7). A similar, albeit smaller, effect was seen for Ile11 H^{N} , which forms an adjacent hydrogen bond to the Cys3 backbone oxygen. This suggests a strengthening of the hydrogen bonds, although a contribution of nearby aromatic rings, in particular of Phe144 (ca. 3 \AA from Cys3 H^{N}) also seems possible. In the six FimH-CRD

Table 2. Thermodynamics of binding of FimH antagonists analyzed by ITC.

Compd	K_{D} [nM]	$\Delta G^{\circ}_{\text{obs}}$ [kJ mol^{-1}]	$\Delta H^{\circ}_{\text{obs}}$ [kJ mol^{-1}]	$-\Delta S^{\circ}_{\text{obs}}$ [kJ mol^{-1}]
1 ^[a]	28.9	-43.0	-50.3	7.3
2 ^[a]	17.7	-44.2	-45.0	0.8
3 ^[b]	3.5	-48.3	-56.2	8.0
4 ^[b]	1.3	-50.7	-60.9	10.1
5 ^[b]	1.0	-51.3	-62.1	10.8
6 ^[a]	14.0	-44.8	-63.6	18.8
7 ^[a]	6.2	-46.8	-71.8	25.0
8 ^[a]	1222	-33.8	-37.2	3.5
9 ^[a]	144	-39.1	-39.1	0.1
10 ^[a]	1125	-34.0	-42.9	9.0
11 ^[a]	89 990	-23.1	-21.1	-2.0

[a] Direct ITC assay format. [b] Competitive ITC assay format with a medium-affinity ligand.

The results indicate that all tested antagonists bind in an enthalpy-driven manner with mostly unfavorable entropic contributions, in accordance with previous studies.^[15d,21,26] The enthalpy term $\Delta H^{\circ}_{\text{obs}} = -42.9\text{ kJ mol}^{-1}$ of 1,5-anhydromannitol (**10**) includes the binding energies from van der Waals contacts and ten specific hydrogen bonds with the protein.^[11] These favorable terms are partly compensated by enthalpic penalties from desolvation of ligand and protein. The enthalpic cost for desolvation of a single hydroxy group had been estimated at 29 kJ mol^{-1} .^[39] On the protein side, X-ray and NMR data and molecular dynamics simulations found evidence of highly structured hydrogen-bonded water in the binding pocket, with this being replaced by the hydroxy groups of the ligand. The classic hydrophobic effect predicts a strong entropic gain for the release of bound water upon complex formation.^[40] However, other studies also suggested an enthalpy-driven “non-classical” hydrophobic effect that is usually explained by water

being forced into an enthalpically unfavorable configuration in the binding pocket.^[41] The entropy term for **10** suggests that any entropic gain from the release of water into the bulk is overcompensated by unfavorable contributions such as the loss of rotational and translational entropy of the ligand (estimated at about 25 kJ mol⁻¹ in aqueous solutions),^[42] as well as by conformational restriction of ligand and protein in the complex. Relevant for the latter is the formation of several hydrogen bonds that reduce the flexibility of the ligand's hydroxy groups and the protein residues involved. Quantification of the individual entropic contributions is cumbersome and in fact still represents a major obstacle in current research.^[41,43]

The thermodynamic data for methyl α -D-mannoside (**8**) reveal a less favorable enthalpy ($\Delta\Delta H^\circ_{\text{obs}}$: 5.7 kJ mol⁻¹) and a smaller entropy penalty ($-T\Delta\Delta S^\circ_{\text{obs}}$: -5.5 kJ mol⁻¹) than in the case of **10**. The additional methoxy group of **8** would be expected to increase the binding enthalpy through van der Waals interactions with the protein (Ile13, Asp47, and Tyr48 within 4 Å). The effective enthalpy loss is due to an additional desolvation penalty for the methoxy group, whereas the entropy gain reflects the release of additional water molecules into the bulk. From NMR CSP experiments we also expect a change in the Tyr48 side chain conformation for all mannosides with methyl or larger aglycones. The implications for the thermodynamics depend on whether the complex formation follows an induced-fit mechanism or conformational selection or a mixture of both.^[28] In a recent solution NMR study of FimH-CRD, ¹⁵N relaxation and CPMG relaxation dispersion experiments investigating the backbone amides did not provide any indication of multiple conformations of Tyr48 in the apo protein, neither of a significant change in the backbone flexibility in the presence of **1**.^[25] The data therefore rather argue for an induced-fit mechanism of the tyrosine gate instead of conformational selection. Nevertheless, conformational equilibria of Tyr48 in the apo state might exist on a timescale not easily accessible by NMR experiments (μs to ms). Hence, the exact binding mechanism remains to be elucidated. Elongation of the aglycone from methyl (compound **8**) to butyl (compound **9**) and heptyl (compound **1**) led to significant improvement in the binding enthalpy, due to the enhanced C–H...π interaction between the elongated alkyl chain and the Tyr48 ring. An expected improvement in the entropy term from the release of more water into the bulk is observed for **9** but not for **1**, which even shows a loss of entropy relative to **8**. We postulated that the stacking interaction of the heptyl chain of **1** with Tyr48 leads to rigidification of both interaction partners and hence to significant entropic costs. For compound **11**, the 4-deoxy-4-fluoro analogue of **1**, a significantly smaller enthalpy term was observed, as would be expected from the disruption of the hydrogen bonds in position 4. The CSP experiments also indicated structural changes in the binding loop containing Tyr137 that can translate into enthalpic costs. Interestingly, the entropy is improved by more than 9 kJ mol⁻¹ relative to **1**, due to the greater flexibility of the protein binding pocket and the ligand.

For the aromatic antagonists **2** to **7**, strongly favorable enthalpy terms ranging from -45.0 to -71.8 kJ mol⁻¹ were ob-

tained. Again, an increase in enthalpy is always accompanied by an increase in entropic costs, as becomes obvious in the enthalpy–entropy compensation plot (Figure S4). X-ray structure data indicate that the outer aromatic rings of antagonists **2** and **4–7** make parallel-displaced π–π interactions with the Tyr48 ring in the *closed* conformation, in analogy to the C–H...π interaction of the heptyl chain of **1**. However, a direct comparison of the thermodynamic data for aliphatic and aromatic antagonists is difficult in view of the large structural difference of the aglycones and because of the many contributing factors. The unsubstituted biphenyl mannoside **2** displayed the smallest enthalpy term and likewise the smallest entropic penalty of all aromatic antagonists. For the substituted biphenyls **3** and **4** we observed significant increases in the enthalpy, by 11.2 and 15.9 kJ mol⁻¹, respectively, relative to **2**. Firstly, the *ortho*-chloro substituent is positioned to enhance the binding enthalpy through favorable van der Waals interactions with the protein in a small pocket formed by Ile52, Tyr137, and Asn138.^[15d] Secondly, the electron-withdrawing character of the substituents allows stronger π–π interaction of the aglycones with Tyr48. As already suggested for the comparison of **1** with **8**, a stronger stacking interaction accounts for a reduced flexibility both in the Tyr48 side chain and in the aglycone, leading to compensating entropic penalties. For antagonist **5**, the enthalpy is slightly better than for the best biphenyl compound **4**. The entropy compensation is only partial, resulting in the strongest dissociation constant of all tested antagonists. Compounds **6** and **7** display the most favorable enthalpies but also the highest entropic penalties. Compound **6** could suffer from entropic costs for rigidification of additional rotatable bonds in the aglycone moiety. Compound **7** is structurally very similar to biphenyl **3** apart from insertion of an amide bond linkage. The dramatically enhanced enthalpy ($\Delta\Delta H^\circ_{\text{obs}}$: -15.6 kJ mol⁻¹) and entropic cost ($-T\Delta\Delta S^\circ_{\text{obs}}$: 17.0 kJ mol⁻¹) of **7** relative to **3** can only be explained in terms of a very efficient stacking interaction with Tyr48 and subsequent loss of conformational entropy in the complex. A comparison of all thermodynamic data demonstrates that the antagonist with the highest enthalpic contribution, presumably from the strongest interaction with Tyr48, is not necessarily the strongest binder. Antagonist **5** exhibits an optimal thermodynamic profile, although its enthalpy term is nearly 10 kJ mol⁻¹ weaker than that of **7**. From the NMR and X-ray data we deduced a distinct orientation of Tyr48 in the presence of **5**, likely as a result of the unique geometry of its indolinylphenyl aglycone. We assume that this complex conformation is optimal in terms of interaction efficiency and minimized compensating entropic penalties.

Conclusion

We have combined NMR chemical shift perturbation (CSP) experiments with high-resolution X-ray structures to elucidate the interaction of the FimH lectin domain with antagonists. One advantage of NMR spectroscopy is its ability to identify even subtle conformational changes of the protein in solution. This is particularly helpful for the determination of ligand bind-

ing modes in cases in which either crystallization was unsuccessful or crystal packing effects distorted the ligand binding site. We demonstrated that the CSP effects of FimH-CRD can be used as an indicator for the conformation of the tyrosine gate motif in the binding pocket. The *open* conformation was observed in the apo protein and with 1,5-anhydromannitol (**10**), whereas antagonists with aliphatic or aromatic aglycones are bound to FimH in the *closed* conformation of the tyrosine gate. The CSP data additionally revealed slight differences in the Tyr48 conformation as a result of different aglycone geometries. Furthermore, the NMR results indicate the presence of highly structured water in the binding pocket of FimH-CRD. In combination with information from crystal structures and molecular modeling, CSP experiments might therefore help to analyze water coordination as an important contributor to the thermodynamics of ligand binding.

We also performed ITC experiments to access full thermodynamic profiles of the antagonists. The results suggest enthalpy–entropy compensation in which enthalpically favorable stacking of hydrophobic aglycones with the Tyr48 side chain leads to conformational restriction of both the protein and the ligand and hence to unfavorable entropy. NMR relaxation experiments with FimH-CRD did not show any changes in the backbone flexibility upon binding of antagonists.^[25] However, we speculate that the flexibility of the protein side chains, in particular of Tyr48, plays a pivotal role in the modulation of FimH–antagonist binding. These effects can be dissected by NMR relaxation experiments for side chain dynamics, and incorporation of the results into rational design might lead to further improved FimH antagonists urgently needed for UTI therapy.

Experimental Section

Protein preparation: FimH-CRD from the *E. coli* K-12 strain was expressed with a C-terminal thrombin cleavage site and a His₆-tag (FimH-CRD-Th-His₆, 173 residues) by a previously published protocol.^[18] The clone containing the FimH-CRD construct was expressed in protease-deficient *E. coli* HM125 at 30 °C and 180 rpm in M9 minimal medium supplemented with MgSO₄ (2 mM), CaCl₂ (0.1 mM), glucose (2 g L⁻¹), and ampicillin (100 µg mL⁻¹). The protein expression was induced by addition of IPTG (1 mM) at an OD₆₀₀ of 0.8. The cells were further cultivated for 16 h and harvested by centrifugation for 20 min at 2000 g and 4 °C. The pellet was resuspended in lysis buffer containing Tris (pH 7.4, 50 mM), NaCl (150 mM), EDTA (5 mM), and polymyxin B sulfate (1 mg mL⁻¹). The supernatant containing the periplasmic extract was dialyzed against sodium phosphate buffer and purified on Ni-NTA columns. For crystallization, the protein without tag was prepared as described in ref. [44] and dialyzed against HEPES buffer (pH 7.4, 20 mM). For production of ¹⁵N- and ¹³C,¹⁵N-labeled FimH-CRD-Th-His₆ for NMR experiments, *E. coli* HM125 was cultivated in M9 minimal medium containing ¹⁵NH₄Cl (1 g L⁻¹) or ¹⁵NH₄Cl (1 g L⁻¹) and ¹³C-glucose (2 g L⁻¹) (Sigma-Aldrich) as the only sources of nitrogen and carbon, respectively. The labeled proteins were purified as described above and dialyzed against phosphate buffer (pH 6.8, 25 mM) in the case of ¹³C,¹⁵N-FimH-CRD-Th-His₆ or phosphate buffer (pH 7.0, 20 mM) in that of ¹⁵N-FimH-CRD-Th-His₆. The purities of the proteins were verified by nonreducing SDS-PAGE analysis,

and the concentrations were determined by UV absorption (Nano-Drop ND-1000, Thermo Scientific). The molecular weights of ¹⁵N-FimH-CRD-Th-His₆ (18860.2 Da) and ¹³C,¹⁵N-FimH-CRD-Th-His₆ (19687.0 Da), determined by mass spectrometry, demonstrated isotope incorporation of >99.9%.

NMR spectroscopy: NMR assignment experiments were performed at 298 K with a Bruker Avance III 700 MHz NMR spectrometer equipped with a 5 mm QCI-P cryogenic probe. A set of triple-resonance NMR spectra of a sample of ¹³C,¹⁵N-FimH-CRD (600 µM) in phosphate buffer (pH 6.8, 25 mM) and H₂O/D₂O (90%/10%) in a 5 mm Shigemi Tube (Shigemi Inc., USA) was recorded for backbone assignment: HNCA, HN(CO)CA, HNCO, HN(CA)CO, HNCACB, and CBCA(CO)NH. Protein stability during data acquisition was tested by regular inspection of 1D ¹H and ¹H,¹⁵N HSQC NMR spectra. Spectra were acquired and processed with Topspin 3.2 (Bruker BioSpin, Switzerland). CcpNmr Analysis (versions 2.2 and 2.3) was used for NMR resonance assignment.^[45] The backbone assignment of FimH-CRD has been deposited in the Biological Magnetic Resonance Data Bank (<http://www.bmrb.wisc.edu>, accession code 26541).

Chemical shift perturbation (CSP) experiments with FimH antagonists were performed with ¹⁵N-FimH-CRD (100 to 200 µM) in non-deuterated phosphate buffer (pH 7.0, 20 mM). FimH antagonists were dissolved in D₂O at 2.5 to 100 mM stock concentrations. Bi-phenyl compound **4** was dissolved at 6.3 mM in D₂O with [D₆]DMSO (40%), due to poor solubility. The antagonists were added at slight molar excesses to ensure complete saturation of the protein. NMR samples were prepared in 3 mm NMR tubes (Hilgenberg, Germany) with 5% D₂O and [D₄]TSP [3-(trimethylsilyl)-2,2',3,3'-tetradecauteropropionic acid, Armar Chemicals, Switzerland] (0.1 mM) added as an internal reference. ¹H,¹⁵N HSQC spectra were measured with a Bruker Avance III 500 MHz spectrometer equipped with a BBO double resonance probe at 298 K. Spectra were acquired and processed with Topspin 2.1 and analyzed with CcpNmr Analysis (versions 2.2 and 2.3).^[45] All antagonists bound in the slow exchange regime, and amide signals of the bound protein were assigned from chemical shift proximity. Combined chemical shift changes of FimH-CRD signals were calculated as weighted averages of ¹H and ¹⁵N chemical shift changes according to Equation (1):^[46]

$$\Delta\delta_{AV} = \sqrt{(\Delta\delta^{1\text{H}^N})^2 + (0.2\Delta\delta^{15\text{N}})^2} \quad (1)$$

Co-crystallization of FimH antagonists: Crystallization of all FimH-CRD/ligand complexes was performed by sitting-drop vapor diffusion. For crystallization trials of ligands **5–7**, FimH-CRD (residues 1–158) was used at a final concentration of 18 mg mL⁻¹ (ca. 1 mM) with a fivefold molar excess of ligand (5 mM) in HEPES buffer (pH 7.4, 20 mM). For crystallization trials with ligand **2**, an FimH-CRD solution (18 mg mL⁻¹) was diluted to 10 mg mL⁻¹ with a saturated solution of ligand **2** in HEPES buffer (pH 7.4, 20 mM). Crystals with ligand **5** were grown as previously described.^[21] Co-crystals with ligand **6** were grown in the Proplex HT-96 screen (Molecular Dimensions, USA) with (NH₄)₂SO₄ (1.5 M) and HEPES (pH 7.0, 0.1 M). After four weeks equilibration at 20 °C, crystals appeared after subsequent equilibration at 4 °C within a few days. Crystals with ligand **7** were grown in PEG 4000 (20%) and NaH₂PO₄ (pH 4.7, 0.2 M) at 20 °C. After two days equilibration, streak seeding with FimH-CRD/**5** co-crystals yielded crystals within 24 h. Crystals with ligand **2** grew within a few days with (NH₄)₂SO₄ (0.2 M), PEG 8000 (19%), and HEPES (pH 7.4, 0.1 M) at 20 °C. All crystals were flash-cooled to 100 K with perfluoropolyether cryo oil (Hampton Re-

search, USA). Data were collected with synchrotron radiation at the PXI (ligand **2**) or PXIII (ligands **5–7**) beamlines of the Swiss Light Source (Paul Scherrer Institute, Switzerland).

Structure determination and refining: Data were indexed, integrated, and scaled with XDS^[47] or iMOSFLM.^[48] Structures were solved by molecular replacement with PHASER^[49] with use of the FimH-CRD-*n*-butyl α-D-mannopyranoside complex (PDB ID: 1UWF^[11a]) as search model. The structures were built by use of the COOT software^[50] and periodically refined with the PHENIX software.^[51] Geometric restraints for the ligands were generated with PRODRG^[52] or Grade Version 1.1.1.^[53] Molprobity^[54] was used to validate the available atomic coordinates and to add protons to PDB files without hydrogens for distance calculation. The structures are deposited in the Protein Data Bank with PDB codes: 4X50 (**2**), 4X5Q (**5**), 4X5R (**6**), and 4X5P (**7**).

Isothermal titration calorimetry (ITC): All ITC experiments were performed with FimH-CRD-Th-His₆ and use of a MicroCal VP-ITC instrument (Malvern Instruments Ltd, Worcestershire, UK) with a sample cell volume of 1.4523 mL. Measurements were performed at 25 °C with a stirring speed of 307 rpm and 10 $\mu\text{cal s}^{-1}$ reference power. The protein was dialyzed against assay buffer [HEPES (10 mM), NaCl (150 mM), pH 7.4]. Injections of ligand solution (3–12 μL) were added at 10 min intervals to a sample cell containing protein (5–50 μM). The *c* values [$c = M_t(0)K_D^{-1}$, where $M_t(0)$ is the initial protein concentration] were in a reliable range between 5 and 1000 for compounds **1**, **2**, and **6–10**. For compounds **3**, **4**, and **5**, the *c* values of the direct titrations were above 1000, so additional competitive ITC experiments were performed.^[38] The ligands were titrated into protein preincubated with an eight- to ninefold excess of compound **12** (structure and synthesis in the Supporting Information), resulting in sigmoidal titration curves. For the low-affinity compound **11** the *c* value was only 0.5, but reliable thermodynamics data could be extracted by fixing the stoichiometry to 1.0. Baseline correction and peak integration was performed with Origin 7 software (OriginLab, USA). Baseline subtraction and curve fitting with the three variables *N* (concentration correction factor), K_D (dissociation constant), and ΔH° (change in enthalpy) were performed with SEDPHAT version 10.40 (National Institutes of Health).^[55] Global fitting to obtain K_D values was performed for the competitive titrations of compound **12** with **3**, **4**, and **5** and for the direct titration of **12**. The ΔH° and *N* values were then obtained by fitting of the direct titrations of **3**, **4**, and **5**. For directly titrated compounds **1**, **2**, and **6–11**, all three variables were determined from a global analysis. The 95% confidence intervals of K_D and ΔH° were calculated with the 1-dimensional error surface projection. The ΔG° and $-T\Delta S^\circ$ (change in entropy) values were calculated from Eq. (2)

$$\Delta G^\circ = \Delta H^\circ - T\Delta S^\circ = -RT \ln K_A \quad (2)$$

with *T* being the absolute temperature and *R* the universal gas constant (8.314 J mol⁻¹ K⁻¹).

Acknowledgements

We sincerely thank Dr. Helene Kovacs of Bruker BioSpin (Fällanden, Switzerland) for acquisition of NMR assignment experiments. B.F. thanks the German Academic Exchange Service (DAAD) for a stipend.

Keywords: FimH • ITC • NMR spectroscopy • urinary tract infections • X-ray diffraction

- [1] B. Foxman, *Am. J. Med.* **2002**, *113 Suppl. 1A*, 55–13S.
- [2] T. J. Wiles, R. R. Kulesus, M. A. Mulvey, *Exp. Mol. Pathol.* **2008**, *85*, 11–19.
- [3] a) G. G. Zhanel, T. L. Hisanaga, N. M. Laing, M. R. DeCorby, K. A. Nichol, B. Weshnoweski, J. Johnson, A. Noreddin, D. E. Low, J. A. Karlosky, N. Group, D. J. Hoban, *Int. J. Antimicrob. Agents* **2006**, *27*, 468–475; b) G. C. Schito, K. G. Naber, H. Botto, J. Palou, T. Mazzei, L. Gualco, A. Marchese, *Int. J. Antimicrob. Agents* **2009**, *34*, 407–413.
- [4] a) N. Sharon, *FEBS Lett.* **1987**, *217*, 145–157; b) E. V. Sokurenko, V. Chesonkova, R. J. Doyle, D. L. Hasty, *J. Biol. Chem.* **1997**, *272*, 17880–17886.
- [5] G. Waksman, S. J. Hultgren, *Nat. Rev. Microbiol.* **2009**, *7*, 765–774.
- [6] I. Le Trong, P. Aprikian, B. A. Kidd, M. Forero-Shelton, V. Tchesnokova, P. Rajagopal, V. Rodriguez, G. Interlandi, R. Klebit, V. Vogel, R. E. Stenkamp, E. V. Sokurenko, W. E. Thomas, *Cell* **2010**, *141*, 645–655.
- [7] G. Zhou, W.-J. Mo, P. Sebbel, G. Min, T. A. Neubert, R. Glockshuber, X.-R. Wu, T.-T. Sun, X.-P. Kong, *J. Cell Sci.* **2001**, *114*, 4095–4103.
- [8] a) I. Ofek, D. L. Hasty, N. Sharon, *FEMS Immunol. Med. Microbiol.* **2003**, *38*, 181–191; b) R. J. Pieters, *Med. Res. Rev.* **2007**, *27*, 796–816.
- [9] M. Aronson, O. Medalia, L. Schori, D. Mirelman, N. Sharon, I. Ofek, *J. Infect. Dis.* **1979**, *139*, 329–332.
- [10] M. Hartmann, T. K. Lindhorst, *Eur. J. Org. Chem.* **2011**, 3583–3609.
- [11] a) J. Bouckaert, J. Berglund, M. Schembri, E. De Genst, L. Cools, M. Wuhrer, C. S. Hung, J. Pinkner, R. Slattegard, A. Zavialov, D. Choudhury, S. Langermann, S. J. Hultgren, L. Wyns, P. Klemm, S. Oscarson, S. D. Knight, H. De Greve, *Mol. Microbiol.* **2005**, *55*, 441–455; b) C. S. Hung, J. Bouckaert, D. Hung, J. Pinkner, C. Widberg, A. DeFusco, C. G. Auguste, R. Strouse, S. Langermann, G. Waksman, S. J. Hultgren, *Mol. Microbiol.* **2002**, *44*, 903–915.
- [12] A. Wellens, C. Garofalo, H. Nguyen, N. Van Gerven, R. Slattegard, J. P. Hernalsteens, L. Wyns, S. Oscarson, H. De Greve, S. Hultgren, J. Bouckaert, *PLoS One* **2008**, *3*, e2040.
- [13] a) N. Firon, S. Ashkenazi, D. Mirelman, I. Ofek, N. Sharon, *Infect. Immun.* **1987**, *55*, 472–476; b) T. K. Lindhorst, C. Kieburg, U. Krallmann-Wenzel, *Glycoconjugate J.* **1998**, *15*, 605–613.
- [14] a) O. Sperling, A. Fuchs, T. K. Lindhorst, *Org. Biomol. Chem.* **2006**, *4*, 3913–3922; b) M. Scharenberg, O. Schwart, S. Rabbani, B. Ernst, *J. Med. Chem.* **2012**, *55*, 9810–9816.
- [15] a) Z. Han, J. S. Pinkner, B. Ford, R. Obermann, W. Nolan, S. A. Wildman, D. Hobbs, T. Ellenberger, C. K. Cusumano, S. J. Hultgren, J. W. Janetka, *J. Med. Chem.* **2010**, *53*, 4779–4792; b) T. Klein, D. Abgottspoon, M. Wittwer, S. Rabbani, J. Herold, X. Jiang, S. Kleeb, C. Luthi, M. Scharenberg, J. Bezencon, E. Gubler, L. Pang, M. Smiesko, B. Cutting, O. Schwart, B. Ernst, *J. Med. Chem.* **2010**, *53*, 8627–8641; c) Z. Han, J. S. Pinkner, B. Ford, E. Chorell, J. M. Crowley, C. K. Cusumano, S. Campbell, J. P. Henderson, S. J. Hultgren, J. W. Janetka, *J. Med. Chem.* **2012**, *55*, 3945–3959; d) L. Pang, S. Kleeb, K. Lemme, S. Rabbani, M. Scharenberg, A. Zalewski, F. Schadler, O. Schwart, B. Ernst, *ChemMedChem* **2012**, *7*, 1404–1422.
- [16] O. Schwart, S. Rabbani, M. Hartmann, D. Abgottspoon, M. Wittwer, S. Kleeb, A. Zalewski, M. Smiesko, B. Cutting, B. Ernst, *Bioorg. Med. Chem.* **2011**, *19*, 6454–6473.
- [17] X. Jiang, D. Abgottspoon, S. Kleeb, S. Rabbani, M. Scharenberg, M. Wittwer, M. Haug, O. Schwart, B. Ernst, *J. Med. Chem.* **2012**, *55*, 4700–4713.
- [18] S. Rabbani, X. Jiang, O. Schwart, B. Ernst, *Anal. Biochem.* **2010**, *407*, 188–195.
- [19] a) D. Abgottspoon, G. Rolli, L. Hosch, A. Steinhuber, X. Jiang, O. Schwart, B. Cutting, M. Smiesko, U. Jenal, B. Ernst, A. Trampuz, *J. Microbiol. Methods* **2010**, *82*, 249–255; b) M. Scharenberg, D. Abgottspoon, E. Cicik, X. Jiang, O. Schwart, S. Rabbani, B. Ernst, *Assay Drug Dev. Technol.* **2011**, *9*, 455–464.
- [20] D. Abgottspoon, B. Ernst, *Chimia* **2012**, *66*, 166–169.
- [21] S. Kleeb, L. Pang, K. Mayer, D. Eris, A. Sigl, R. C. Preston, P. Zihlmann, T. Sharpe, R. P. Jakob, D. Abgottspoon, A. S. Hutter, M. Scharenberg, X. Jiang, G. Navarra, S. Rabbani, M. Smiesko, N. Ludin, J. Bezencon, O. Schwart, T. Maier, B. Ernst, *J. Med. Chem.* **2015**, *58*, 2221–2239.

- [22] a) A. Cléry, M. Schubert, F. H. Allain, *Chimia* **2012**, *66*, 741–746; b) M. del Carmen Fernandez-Alonso, D. Diaz, M. A. Berbis, F. Marcelo, J. Canada, J. Jimenez-Barbero, *Curr. Protein Pept. Sci.* **2012**, *13*, 816–830.
- [23] a) S. B. Shuker, P. J. Hajduk, R. P. Meadows, S. W. Fesik, *Science* **1996**, *274*, 1531–1534; b) L. Skjærven, L. Codutti, A. Angelini, M. Grimaldi, D. Latek, P. Monecke, M. K. Dreyer, T. Carlomagno, *J. Am. Chem. Soc.* **2013**, *135*, 5819–5827.
- [24] a) G. Wagner, A. Pardi, K. Wuthrich, *J. Am. Chem. Soc.* **1983**, *105*, 5948–5949; b) M. P. Williamson, *Prog. Nucl. Magn. Reson. Spectrosc.* **2013**, *73*, 1–16.
- [25] S. Vanwetswinkel, A. N. Volkov, Y. G. Sterckx, A. Garcia-Pino, L. Buts, W. F. Vranken, J. Bouckaert, R. Roy, L. Wyns, N. A. van Nuland, *J. Med. Chem.* **2014**, *57*, 1416–1427.
- [26] A. Wellens, M. Lahmann, M. Touaibia, J. Vaucher, S. Oscarson, R. Roy, H. Remaut, J. Bouckaert, *Biochemistry* **2012**, *51*, 4790–4799.
- [27] G. Roos, A. Wellens, M. Touaibia, N. Yamakawa, P. Geerlings, R. Roy, L. Wyns, J. Bouckaert, *ACS Med. Chem. Lett.* **2013**, *4*, 1085–1090.
- [28] D. D. Boehr, R. Nussinov, P. E. Wright, *Nat. Chem. Biol.* **2009**, *5*, 789–796.
- [29] D. Choudhury, A. Thompson, V. Stojanoff, S. Langermann, J. Pinkner, S. J. Hultgren, S. D. Knight, *Science* **1999**, *285*, 1061–1066.
- [30] M. Sattler, J. Schleucher, C. Griesinger, *Prog. Nucl. Magn. Reson. Spectrosc.* **1999**, *34*, 93–158.
- [31] The backbone resonance assignment was deposited in the Biological Magnetic Resonance Database (BMRB) entry: 26541.
- [32] M. Scharenberg, X. Jiang, L. Pang, G. Navarra, S. Rabbani, F. Binder, O. Schwardt, B. Ernst, *ChemMedChem* **2014**, *9*, 78–83.
- [33] M. J. Cloninger, H. W. Whitlock, *J. Org. Chem.* **1998**, *63*, 6153–6159.
- [34] E. A. Meyer, R. K. Castellano, F. Diederich, *Angew. Chem. Int. Ed.* **2003**, *42*, 1210–1250; *Angew. Chem.* **2003**, *115*, 1244–1287.
- [35] A. Zalewski, PhD thesis, University of Basel (Basel), **2013**.
- [36] V. B. Rodriguez, B. A. Kidd, G. Interlandi, V. Tchesnokova, E. V. Sokurenko, W. E. Thomas, *J. Biol. Chem.* **2013**, *288*, 24128–24139.
- [37] D. W. Cruickshank, *Acta Crystallogr. Sect. D Biol. Crystallogr.* **1999**, *55*, 583–601.
- [38] B. W. Sigurskjold, *Anal. Biochem.* **2000**, *277*, 260–266.
- [39] a) L. Frick, C. Yang, V. E. Marquez, R. Wolfenden, *Biochemistry* **1989**, *28*, 9423–9430; b) W. M. Kati, R. Wolfenden, *Biochemistry* **1989**, *28*, 7919–7927.
- [40] R. U. Lemieux, *Acc. Chem. Res.* **1996**, *29*, 373–380.
- [41] a) J. M. Myslinski, J. E. DeLorbe, J. H. Clements, S. F. Martin, *J. Am. Chem. Soc.* **2011**, *133*, 18518–18521; b) K. L. Portman, J. Long, S. Carr, L. Briand, D. J. Winzor, M. S. Searle, D. J. Scott, *Biochemistry* **2014**, *53*, 2371–2379; c) P. W. Snyder, J. Mecinovic, D. T. Moustakas, S. W. Thomas 3rd, M. Harder, E. T. Mack, M. R. Lockett, A. Heroux, W. Sherman, G. M. Whitesides, *Proc. Natl. Acad. Sci. USA* **2011**, *108*, 17889–17894.
- [42] a) J. J. Lundquist, E. J. Toone, *Chem. Rev.* **2002**, *102*, 555–578; b) W. B. Turnbull, B. L. Precious, S. W. Homans, *J. Am. Chem. Soc.* **2004**, *126*, 1047–1054.
- [43] M. Ambrosi, N. R. Cameron, B. G. Davis, *Org. Biomol. Chem.* **2005**, *3*, 1593–1608.
- [44] M. Vetsch, P. Sebbel, R. Glockshuber, *J. Mol. Biol.* **2002**, *322*, 827–840.
- [45] W. F. Vranken, W. Boucher, T. J. Stevens, R. H. Fogh, A. Pajon, M. Llinas, E. L. Ulrich, J. L. Markley, J. Ionides, E. D. Laue, *Proteins Struct. Funct. Bioinf.* **2005**, *59*, 687–696.
- [46] M. Pellecchia, P. Sebbel, U. Hermanns, K. Wuthrich, R. Glockshuber, *Nat. Struct. Biol.* **1999**, *6*, 336–339.
- [47] a) W. Kabsch, *Acta Crystallogr. Sect. D Biol. Crystallogr.* **2010**, *66*, 133–144; b) W. Kabsch, *Acta Crystallogr. Sect. D Biol. Crystallogr.* **2010**, *66*, 125–132.
- [48] T. G. Battye, L. Kontogiannis, O. Johnson, H. R. Powell, A. G. Leslie, *Acta Crystallogr. Sect. D Biol. Crystallogr.* **2011**, *67*, 271–281.
- [49] A. J. McCoy, *Acta Crystallogr. Sect. D Biol. Crystallogr.* **2007**, *63*, 32–41.
- [50] P. Emsley, K. Cowtan, *Acta Crystallogr. Sect. D Biol. Crystallogr.* **2004**, *60*, 2126–2132.
- [51] P. D. Adams, P. V. Afonine, G. Bunkoczi, V. B. Chen, I. W. Davis, N. Echols, J. J. Headd, L. W. Hung, G. J. Kapral, R. W. Grosse-Kunstleve, A. J. McCoy, N. W. Moriarty, R. Oeffner, R. J. Read, D. C. Richardson, J. S. Richardson, T. C. Terwilliger, P. H. Zwart, *Acta Crystallogr. Sect. D Biol. Crystallogr.* **2010**, *66*, 213–221.
- [52] D. M. van Aalten, R. Bywater, J. B. Findlay, M. Hendlich, R. W. Hooft, G. Vriend, *J. Comput. Aided Mol. Des.* **1996**, *10*, 255–262.
- [53] O. S. Smart, T. O. Womack, A. Sharff, C. Flensburg, P. Keller, W. Paciorek, C. Vonrhein, G. Bricogne, Grade Version 1.1.1, Copyright by Global Phasing Limited, **2011**.
- [54] V. B. Chen, W. B. Arendall III, J. J. Headd, D. A. Keedy, R. M. Immormino, G. J. Kapral, L. W. Murray, J. S. Richardson, D. C. Richardson, *Acta Crystallogr. Sect. D Biol. Crystallogr.* **2010**, *66*, 12–21.
- [55] J. C. Houtman, P. H. Brown, B. Bowden, H. Yamaguchi, E. Appella, L. E. Samelson, P. Schuck, *Protein Sci.* **2007**, *16*, 30–42.

Manuscript received: December 23, 2014

Final article published: May 4, 2015